Stochastic Joint Simulation of Facies and Diagenesis: A Case Study on Early Diagenesis of the Madison Formation (Wyoming, USA).

M. Barbier, Youri Hamon, Brigitte Doligez, Jean-Paul Callot, M. Floquet, Jean-Marc Daniel

Oil & Gas Science and Technology – Rev. IFP Energies nouvelles, Vol. 67 (2012), No. 1, pp. 123-145

DOI: 10.2516/ogst/2011009

Dossier

Diagenesis - Fluid-Rocks Interactions
Diagenèse minérale - Équilibres fluides-roches

Stochastic Joint Simulation of Facies and Diagenesis: A Case Study on Early Diagenesis of the Madison Formation (Wyoming, USA)

M. Barbier[1,2], Y. Hamon[1*], B. Doligez[1], J.-P. Callot[1], M. Floquet[2] and J.-M. Daniel[1]

1 IFP Energies nouvelles, 1-4 avenue de Bois-Préau, 92852 Rueil-Malmaison - France
2 Laboratoire de Géologie des Systèmes et Réservoirs Carbonatés, EA 4234, Université de Provence, 3 place Victor Hugo, 13003 Marseille - France
e-mail: mickael.barbier@ifpen.fr - youri.hamon@ifpen.fr - brigitte.doligez@ifpen.fr - jean-paul.callot@ifpen.fr marc.floquet@up.univ-mrs.fr - jean-marc.daniel@ifpen.fr

* Corresponding author

Résumé — Simulation stochastique couplée faciès et diagenèse. L'exemple de la diagenèse précoce dans la Formation Madison (Wyoming, USA) — Nous proposons dans cet article une approche intégrée visant à reproduire à la fois les faciès sédimentaires et les phases diagénétiques associées, au sein d'un modèle statique de réservoir. Dans le Wyoming (USA), la Formation Madison (d'âge Mississippien) est une formation carbonatée, épaisse de 200 à 350 m, affleurant dans plusieurs zones du bassin d'avant-pays des Bighorn.

Au sein de cette série, nous avons identifié neuf faciès sédimentaires, groupés en trois séquences de faciès (basées sur l'empilement vertical des faciès): 1) une séquence inter- à supratidale; 2) une séquence subtidale peu profonde à intertidale; 3) une séquence subtidale profonde et ouverte. Ces faciès ont ensuite été intégrés au sein d'un modèle de dépôts synthétique, correspondant à une rampe carbonatée évoluant graduellement vers une géométrie de plate-forme dont seule la partie la plus interne est reconnue. Ce travail a permis de proposer un cadre chronostratigraphique pour la série, qui couvre au moins six séquences de dépôts de troisième ordre (certaines d'entre elles étant localement absentes car érodées).

L'étude de la diagenèse s'est concentrée sur l'identification et la succession des phases diagénétiques précoces (micritisation, cimentation calcitique, dolomitisation, etc.). Pour les besoins de la modélisation, sept « empreintes diagénétiques » ont été définies, chacune d'entre elles correspondant à une succession de phases diagénétiques coexistant au sein d'un même faciès sédimentaire. De plus, nous avons quantifié la proportion relative de chaque empreinte diagénétique affectant un faciès sédimentaire.

Un modèle maillé 3D a alors été bâti afin de reproduire l'organisation des faciès des trois premières séquences de dépôts (qui sont les mieux documentées). Le maillage est donc basé sur les quatre limites de séquences reconnues sur toutes les coupes. Les relations entre faciès sédimentaires et diagenèse ont été utilisées pour définir les paramètres de simulation. Ces dernières sont basées sur des algorithmes plurigaussien et emboîtés. Finalement, nous proposons une discussion sur la distribution des hétérogénéités réservoirs potentielles, prenant en compte à la fois les caractéristiques sédimentaires (faciès, architecture, continuité latérale, etc.) mais également l'impact de la diagenèse.

Abstract — Stochastic Joint Simulation of Facies and Diagenesis: A Case Study on Early Diagenesis of the Madison Formation (Wyoming, USA) — *The aim of this paper is to propose an integrated approach to reproduce both facies and diagenetic trends in a static reservoir model based on an outcrop* *case study. In Wyoming (USA), the Madison Formation (Mississippian) is a thick (up to 350 m) carbonate series, outcropping in several locations of the Bighorn foreland basin.*

Within these series, nine sedimentary facies have been identified. Based on their vertical stacking pattern, they are organized in small-scale facies sequences: 1) intertidal to supratidal facies sequence; 2) shallow subtidal to intertidal facies sequence; 3) deep subtidal facies sequence. These facies associations have been integrated in a synthetic depositional model, which corresponds to a carbonate ramp progressively evolving towards the most inner part of a platform. This enables to propose a sequence stratigraphy framework for the studied series, that represents at least six third-order sequences (some of them being locally eroded).

The diagenetic study has been focused on the identification of the early diagenetic phases. Results from these analyses show the occurrence of several successive early diagenetic phases (micritization, marine calcite cementation, dolomitization, etc.). For modeling purposes, seven "diagenetic imprints" have been defined, each of them corresponding to a succession of diagenetic phases that can coexist in the same sedimentary facies. Moreover, as each sedimentary facies may be affected by several diagenetic imprints, a quantification of these imprints has been realized.

A 3D gridded model designed for geostatistical modeling has been constructed in order to reproduce the facies organization of the three first third-order sequences (that are the best documented). The gridding is then based on the four sequence boundaries which have been recognized on every section. The relationships between sedimentary facies and diagenesis have been used to define lithofacies simulation rules. The simulations are based on the plurigaussian and nested algorithms. Finally, a discussion on the distribution of the potential reservoir heterogeneities is proposed, taking into account the sedimentary characteristics (facies, architectures, etc.) and the diagenetic impact.

INTRODUCTION

Carbonate reservoir properties are controlled primarily by the sedimentary facies, and are strongly modified by its diagenetic history, early or late (Lézin *et al*., 2009). This two parameters may subsequently influence the development of the fracture network (*e.g*. Laubach *et al*., 2009), that may act either as fluid flow drain and/or barrier and thus conversely control the late diagenetic processes. In short, diagenesis increases the complexity to characterize and further to model the carbonate reservoirs (Shackelton *et al*., 2005; Olson *et al*., 2007; Wennberg *et al*., 2006). A new challenge for carbonate reservoir characterization is thus to model diagenesis and the derived reservoir heterogeneities.

A large number of works has already been published on this topic, following different approaches. Forward modeling have been used by Whitaker *et al*. (1997) and Patterson *et al*. (2008), to model an early meteoric diagenesis occurring on an isolated carbonate platform. The reactive transport modeling has been used for modeling of various type of dolomitization (Caspard *et al*., 2004; Salas *et al*., 2007; see also Steefel and MacQuarrie, 1996, and Consonni *et al*., 2010 for updated summaries), calcite dissolution by mixing of fresh and marine waters (Rezaei *et al*., 2005), dedolomitization (Ayora *et al*., 1998) or illitization (Le Gallo *et al*., 1998). Thus, reactive-transport modeling applied to carbonate systems is a relatively young discipline (last decade). Even if it has been successfully tested to predict the distribution of diagenetic processes (Xiao et Jones, 2006), it is still an ongoing research topic that aims to validate conceptual diagenetic models based on the diagenetic analyses or discuss the influence of the factors involved in a diagenetic process (Whitaker *et al*., 2004).

Carbonate sedimentary facies and their related reservoir heterogeneities can also be modeled with geostatistical approaches. A wide range of methods and algorithms have been developed in the past (indicator simulations, truncated Gaussian simulations, boolean or object-based simulations; Haldorsen and Damsleth, 1990; Lantuéjoul, 2001; Matheron *et al*., 1987; Ravenne *et al*., 2000) up to advanced geostatistical techniques, such as nested, plurigaussian and bi-plurigaussian simulations (Doligez *et al*., 2009; Dowd *et al*., 2003; Emery, 2007; Normando *et al*., 2005 among others). However, such facies models often reproduce the reservoir petrophysical properties incompletely, as the diagenetic events that modify porosity and permeability are not integrated. Indeed, only a few articles have been published on the use of geostatistical modeling to reproduce diagenetic trends (Le Loc'h and Galli, 1996; Labourdette, 2007).

Thus, the aim of this paper is to apply the complete workflow from data acquisition to geostatistical modeling of both facies and diagenesis (plurigaussian and nested methods), on a case study: the Madison Formation (Mississippian in age) of the Bighorn Basin (Wyoming, USA). This paper will be only focused on the early diagenesis that presents an important variability and a direct link to the sedimentary environment (and thus the sedimentary facies). The workflow (that constitute the outline of the article) is composed of a sedimentological characterization (facies description and interpretation), associated with a detailed diagenetic identification and description of the early phases of diagenesis that affected these series. These results are in turn used to propose a modeling workflow, which integrates the diagenetic constraints in a pre-existing stochastic facies simulation.

1 GEOLOGICAL SETTING

1.1 Structural Setting

The study area is located in the Northern part of the Bighorn Basin (Wyoming), on the edge of the Rocky Mountains. The Bighorn Basin is separating the Rocky Mountains to the West from the Bighorn Mountains to the East and the Wind River Uplift to the South *(Fig. 1a)*. During Early Mississippian, at the western part of the North American Continent, the Antler Orogeny formed the Antler Mountains and the associated foreland basin to the West and an intra-continental shelf to the East, upon which the Madison Formation developed *(Fig. 1b, c)*. These latter series were buried until the Cretaceous. Subsequently, two compressive shortening stages occurred throughout the western United States during the building of the North American Cordillera. In Wyoming, the far stress field of the Sevier Orogeny tectonic phase is associated to thin skin deformation during the Cretaceous (120 to 65 Ma). It involved mostly the formation of microstructures within the Bighorn Basin, associated to an EW to N110 compressive stress direction locally disturbed to N130 along the incipient Sheep Mountain fold. Secondly, the compressive Laramide Orogeny is responsible of a thick skin inversion of deeper structures, in particular the NW-SE basement arches such as the Sheep Mountain Anticline or the Bighorn Mountains, where the Shell Canyon outcrop is located (Amrouch *et al.*, 2010; Neely and Erslev, 2009; Stanton and Erslev, 2004).

1.2 Paleogeographic and Stratigraphic Settings

The Madison Formation has been deposited during the Early Mississippian (357 to 340 Ma) on a shallow water carbonate shelf, located ~5°N of the palaeo-equator and extending approximately 1600 km long and 400 km wide from New Mexico to Western Canada (Gutschick *et al.*, 1983; Sonnenfeld, 1996). The shelf was bounded to the North by the Central Montana Trough and the Williston Basin, to the West by the Antler Mountain Arc and foreland basin and to the South-Southeast by the Transcontinental Arch that was probably the main source of siliciclastic sediments during the Early Mississippian *(Fig. 1b)*. The Madison Formation thickens irregularly from the South-East to the North-West and can reach more than 400 m at the North-western border of the Bighorn Basin.

The Madison Formation corresponds to a second-order depositional sequence, constituted of six third-order sequences, composed themselves of higher frequency cycles *sensu* Elrick and Read (1991), Reid *et al.* (1993) *(Fig. 2)*. Our study concerns the three lower third-order sequences which correspond to the Little Bighorn, Woodhurst and Big Goose Members *(Fig. 2)*. According to Sonnenfeld (1996), the two first sequences were deposited along a homoclinal ramp exhibiting regional progradational geometry throughout the Wyoming, while the third to sixth third-order sequences were deposited on a flat-topped platform dominated by restricted lagoonal and evaporitic conditions. Each of these third-order sequences is bounded by solution collapse breccias that can be used as correlation guidelines throughout a proximal-distal transect (Westphal *et al.*, 2004). Finally, at the end of the Mississippian, the Madison Formation is affected by a long period of subaerial exposure (10 to 12 Ma of duration) creating sinkholes, solution-collapse breccias, and cavities (Sando, 1988).

2 METHODOLOGY AND DATASET

The sedimentological and diagenetic descriptions have been made on five detailed sedimentological sections located all over the Bighorn Basin (Sheep Mountain backlimb and forelimb, Shell Canyon, Wind River, Shoshone Canyon). Each of these sections has been described at the 1/100 scale. However, as they are too much scattered on the whole Bighorn Basin (which is 250 by 200 km in size), only a part of this basin has been considered for modeling, using the Shell Canyon section and two sections in Sheep Mountain (both the backlimb and forelimb) as direct inputs. Two other sections were used for the modeling part, corresponding to well data (Garland Field and Torchlight Field) and based on the descriptions made by Sonnenfeld (1996), consistent with ours.

About 200 thin sections (made from oriented plugs, sampled with a semi systematic method, a sample every meter with specific focus in case of local, small scale facies variations) were thoroughly analyzed for faciologic and diagenetic purposes. All thin sections have been stained with alizarin red-S and potassium ferricyanide (Dickson, 1966) to differentiate carbonate minerals (aragonite and calcite are stained, while dolomite remains unstained) and distribution of ferrous iron. Petrographic observations included conventional and cathodoluminescence (CL) microscopy (Technosyn Cold CL Model 8200 Mark II, Technosyn Corp., Cambridge, MA, USA; operation conditions were 16-20 kV gun potential, 420-600 μA beam current, 0.05 Torr vacuum and 5 mm beam width; and OPEA system, OPEA France; operation conditions 12-14 kV gun potential).

The various diagenetic phases were carefully sampled (using a dentist micro-drill) in order to analyze their carbon and oxygen stable isotopic composition. Carbonate powders were reacted with 100% phosphoric acid (density

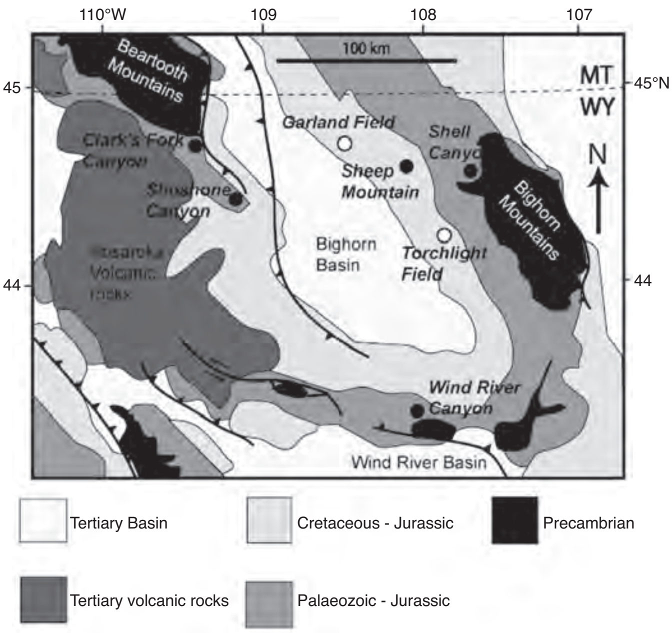

a)

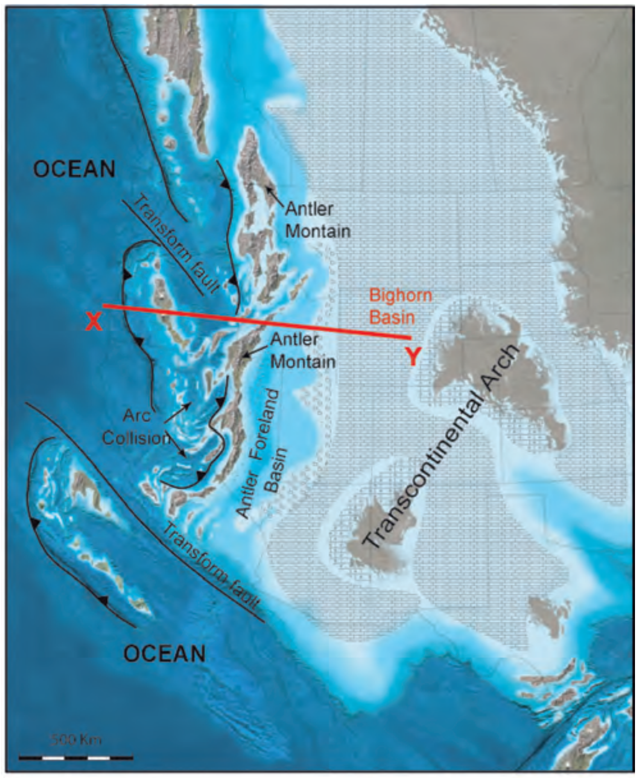

b)

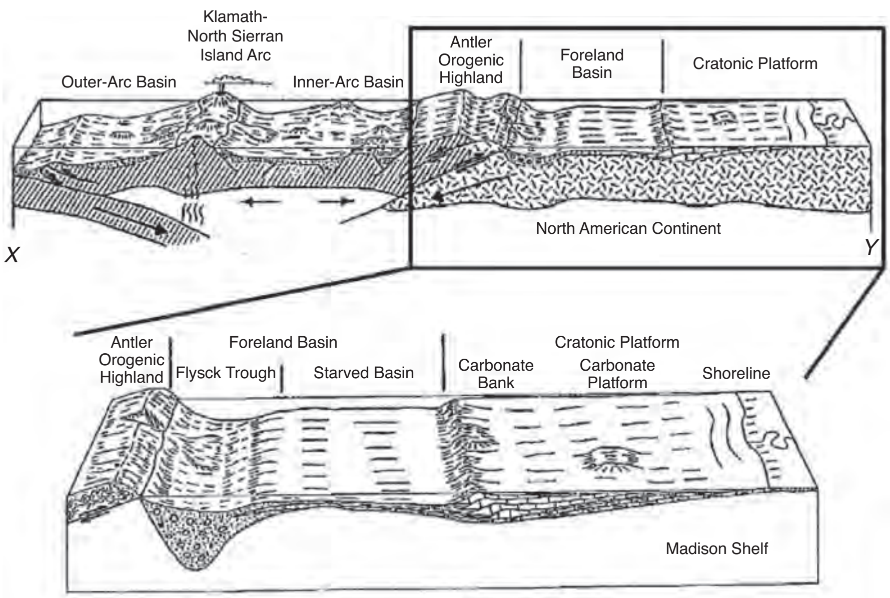

c)

Figure 1

a) Simplified geological map of the Bighorn Basin, showing the location of the studied sections and wells (black dot for field sections, white dot for wells).

b) Regional paleogeography of the Western United States (Modified from R. Blakey's personal webpage). XY section corresponds to Figure 1c.

c) Hypothetical and generalized diagram showing relation between latest Devonian and Mississipian island-arc system and North-American continent during Antler orogenic deformation. A closer view shows the depositional settings of foreland basin and cratonic shelf (from Poole *et al.*, 1977).

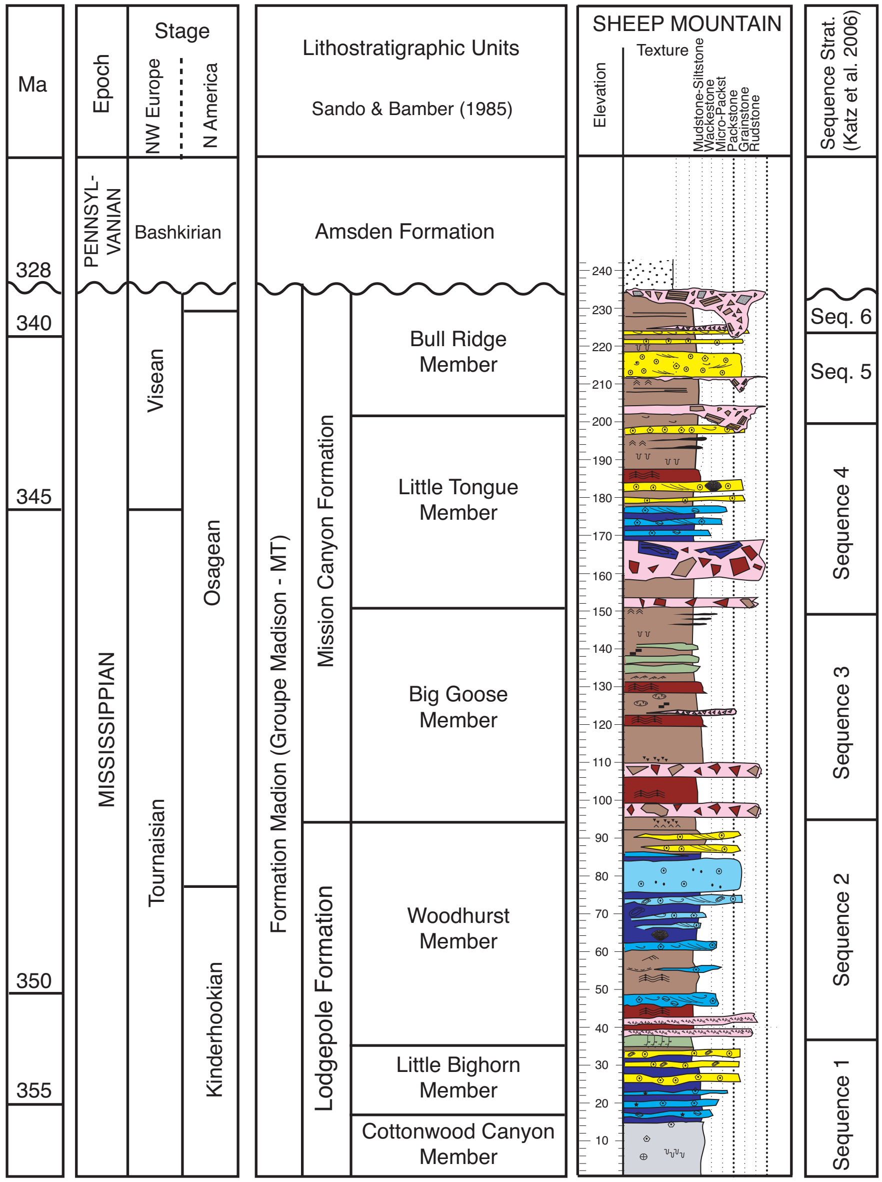

Figure 2

Lithostratigraphy of the Madison Formation in the Bighorn Basin. Equivalent North-American and European stages are given for the lithostratigraphic members of the Madison Formation (from Sando and Bamber, 1985). At right, the synthetic sedimentary log from this study of the Madison Formation at Sheep Mountain and the corresponding sequence stratigraphy (modified from Katz *et al*., 2006) are given.

>1.9, Wachter and Hayes, 1985) at 75°C using a Kiel III online carbonate preparation line connected to a ThermoFinnigan 252 mass-spectrometer. All values are reported in per mil relative to Vienna Pee Dee Belemnite standard (V-PDB) by assigning a $\delta^{13}C$ value of +1.95‰ and a $\delta^{18}O$ value of −2.20‰ to NBS19 (reference number of the internationally distributed reference material calcite). Oxygen isotopic compositions of dolomite were corrected using the fractionation factors given by Rosenbaum and Sheppard (1986). Reproducibility was checked by replicated analysis of laboratory standards. It is better than ±0.02‰ (1σ) and can be considered as very good.

3 SEDIMENTOLOGICAL CHARACTERIZATION

3.1 Sedimentary Facies Characterization

Facies analysis is based on macroscopic and microscopic descriptions. Nine facies *(Tab. 1)* have been defined by texture, sediment constituents, sedimentary structures and fossil

TABLE 1

Facies and facies association description

Lithofacies + Thickness	Lithology / Texture	Sedimentary structures	Skeletal allochems	Non-skeletal allochems	Interpretation
Intertidal to supratidal facies association					
Evaporite solution collapse breccias (F1) (0.1-0.5 m)	Breccias with a dolomicritic to dolomicrosparitic matrix (97% of dolomite and 3% of silica)	- Lenticular bodies - Pseudomorphoses of evaporites - Some cherts	None	Monogenic centimetre-scale angular clasts	Subaerially exposed supratidal environments
Mudstone with root traces (F2) (0.5 m)	Mudstone (100% limestone)	- Root traces and gypsum pseudomorphoses	None	None	Supratidal to intertidal environment
Stromatolithes (F3) (0.2-1 m)	Dolomudstone (100% dolomite)	- Millimetre-scale planar or undulating millimetre-thick laminae of dolomicrite and dolomicrosparite, forming dark/light alternations - Rare bioturbations	None	Brecciated laminae (flat pebbles) at top of beds	Supratidal to upper intertidal environment
Intraclastic / peloidal wackestone (F4) (0.2-1.5 m)	Wackestone with a dolomicritic to dolomicrosparitic matrix	- Oscillation and current ripples - Some almond shaped cherts - Common escape burrows	Solitary corals	Intraclasts and peloids	Shallow lower intertidal environment
Shallow subtidal to intertidal shoal facies association					
Oolitic grainstone (F5) (0.2-1.6 m)	Grainstone (100% limestone)	- Erosive bases, cross-bedded laminations and wave ripples	None	More than 70% of ooids, peloids (30%)	2D-3D mobile sand dunes in a shallow lower subtidal environment
Poorly sorted bioclastic grainstone to packstone (F6) (0.1-2 m)	Grainstone to packstone (matrix is dolomitized in packstone)	- Erosive bases and lag of reworked intraclasts at the base - HCS. Lens shape	Brachiopods (10%), crinoid fragments (47%) and rare solitary corals and oyster fragments. Micritization	Ooids (5%), intraclasts (38%). Intense micritization	Storm deposits in a shallow subtidal environment
Subtidal to intertidal shoal facies association					
Intraclastic rudstone to grainstone (F7) (0.3-1 m)	Rudstone to grainstone (matrix is dolomitized in rudstone)	- Erosive bases and lag of reworked intraclasts at the base - Lens shape	Crinoids (9%). Other various bioclasts	More than 70% of intraclasts and micritized oncoids, peloids (11%), ooids (9%)	Hydraulic dune complexes in a deeper subtidal environment
Crinoidal dolowackestone (F8) (0.2-1 m)	Dolomitized wackestone (95% dolomite)	- Common burrows at tops of beds - Rare stratiform cherts - Burrows at tops of beds	Crinoids, brachiopods (Spirifera) and some solitary corals (Rugosa Zaphrentis)	Peloids	Deep subtidal, low energy environment
Bioturbated. dolomudstone (F9) (> 1 m)	Dolomudstone (100% dolomicrosparite)	- Intense bioturbation.	Rare crinoids, rare brachipods, and some solitary corals.	None.	Deep subtidal low . energy environment

and/or trace fossil content (where present). Subsequently, they were grouped into three facies associations, attributed to a specific depositional environment *(Tab. 1)*. This interpretation has been made according to the tidal zonation (supratidal to subtidal environments), on the basis of their constituent facies, packaging patterns and overall geometry (analyzed from 2D outcrops at the cliffs in the Sheep Mountain Anticline).

In this succession, small-scale facies sequences (0.3 to 3 m in thickness) can be identified, based on the vertical facies arrangement and features of bounding surfaces. Three types of facies sequences are thus recognized: intertidal to supratidal sequence; shallow subtidal to intertidal sequence; subtidal sequence. They roughly correspond to the “cycles” defined by Elrick and Read (1991). They will be used as direct input in the modeling workflow, to build the lithotype rules that are supposed to represent the vertical and the spatial facies arrangement *(Fig. 3)*.

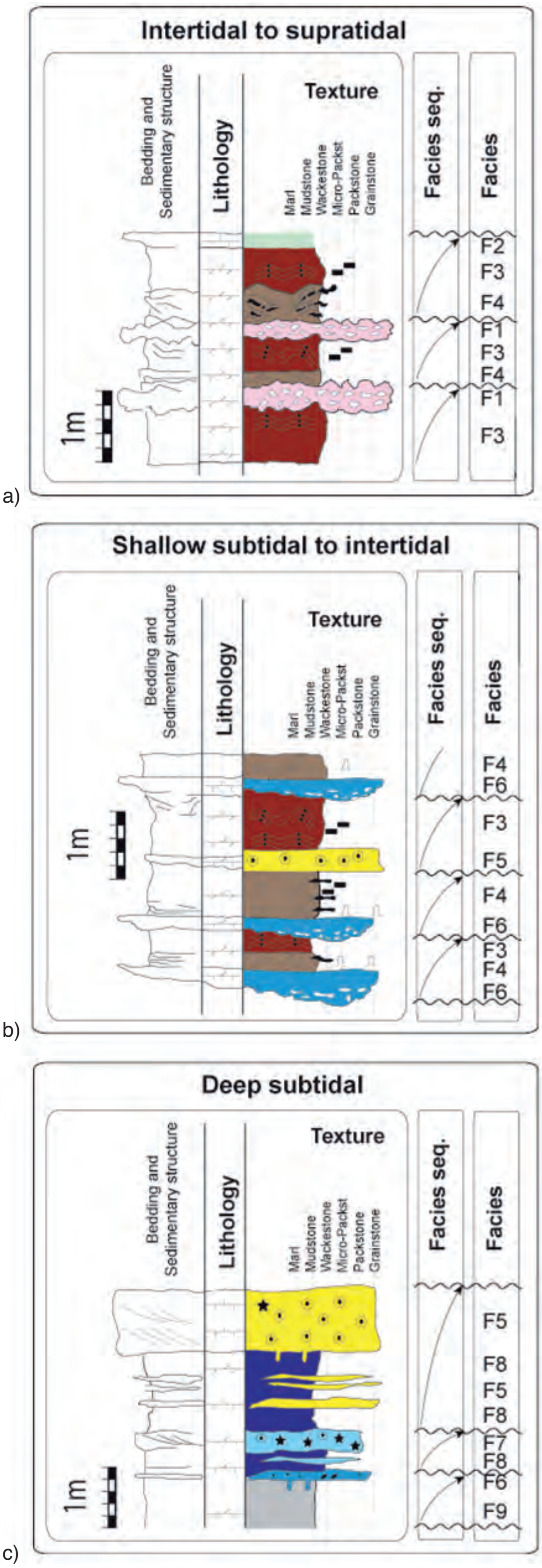

Figure 3

Facies sequence type observed within the studied sections based on the vertical facies arrangement and features of bounding surfaces. Color and symbol code in Figure 6.

3.1.1 Intertidal to Supratidal Facies Sequence

3.1.1.1 Description

This type of sequence is composed of four different facies:

- facies F1, an evaporitic solution collapse breccia, organized in centimetric to metric beds, and formed of angular clasts in a dolomicritic matrix and presenting pseudomorphoses of anhydrite *(Fig. 4a)*;
- facies F2 that corresponds to a mudstone with root traces *(Fig. 4b)* and silicified pseudomorphoses of gypsum;
- facies F3, a dolomicrite to dolomicrosparite, with planar or undulating millimetre-thick laminae, which are sometimes broken by desiccation and form centimetre-scale angular intraclasts (flat pebbles; *Fig. 4c, d*);
- facies F4, an intraclastic dolowackestone, sometimes burrowed, showing centimetric laminae with oscillation and current ripples *(Fig. 4e, f)*. Peloids and solitary corals are also common.

A typical intertidal-supratidal facies *(Fig. 3a)* generally begins with the facies F4, passing upward to the facies F3 (absent in certain case), and are finally capped either by the facies F1 or the facies F2.

3.1.1.2 Interpretation

Absence of desiccation features in the intraclastic dolowackestones (F4) and small-scale oscillation ripples point to a shallow intertidal depositional environment (Tucker and Wright, 1990). On the basis of many modern examples, algal laminites facies (F3) are considered to have formed in supratidal to upper intertidal environments (Hardie and Shinn, 1986; Tucker and Wright, 1990). Moreover, the presence of reworked flat pebbles associated to the laminites may evidence subaerial exposure conditions. In the same way, the presence and the preservation of root traces (F2) suggest an early lithification associated to a supratidal environment. Evaporite pseudomorphoses are clearly indicative of a supratidal environment under arid conditions (Warren, 2006). Evaporite precipitation may have involved the dolomitization of the surrounding and underlying sediments, and their dissolution may have generated collapses and formation of the breccias (Warren, 2006). It is unclear if the water that dissolves these evaporites was fresh or marine water.

These intertidal to supratidal facies sequences thus correspond to shallowing-upward trends, owing to the filling of the available space by the carbonate sedimentation and final sulphate precipitation. Positive accommodation allowed to create new available space for sedimentation and to stack up such sequences.

3.1.2 Shallow Subtidal to Intertidal Facies Sequence

3.1.2.1 Description

This facies sequence is composed of four facies:

- facies F3 (algal laminites facies);

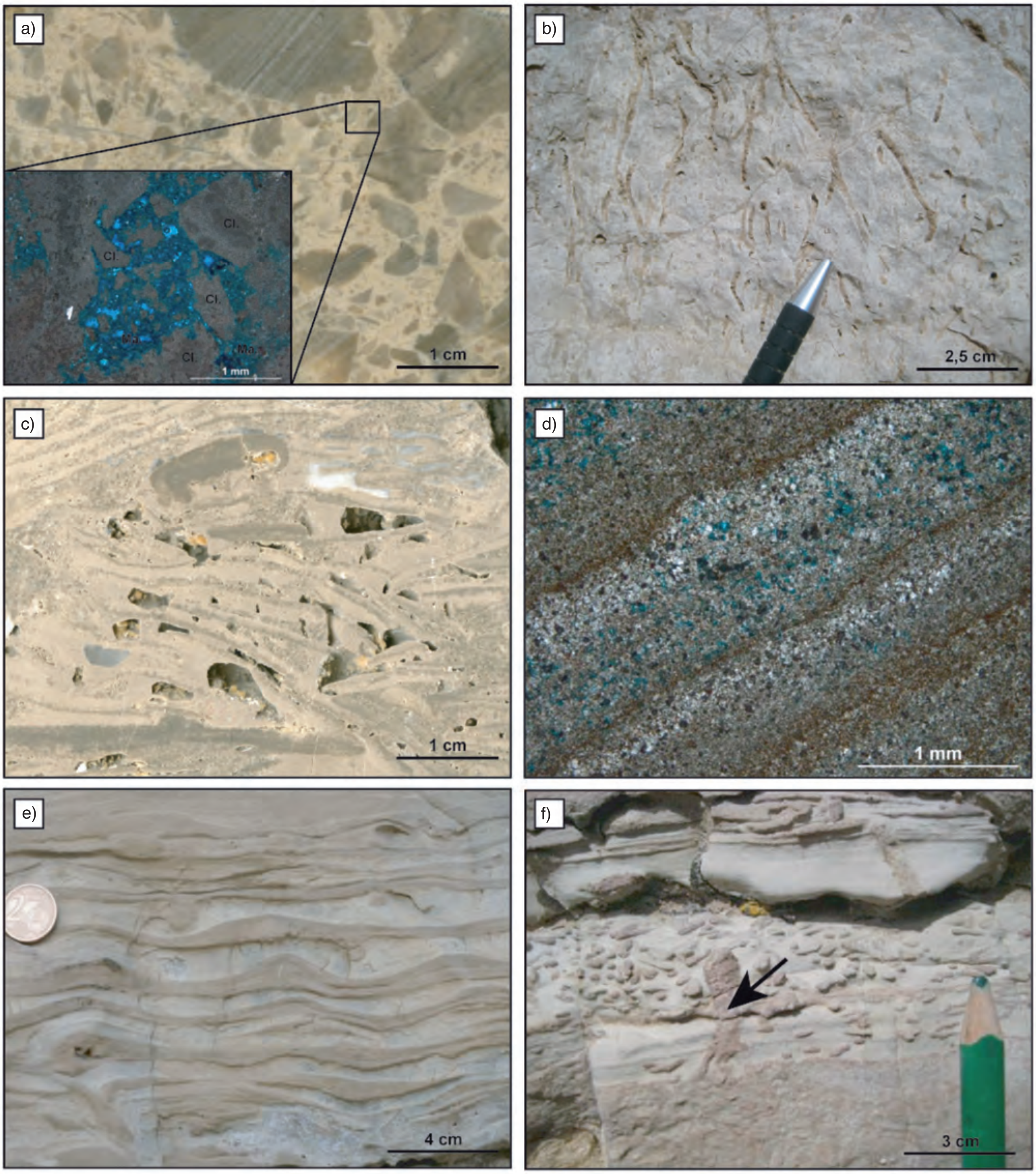

Figure 4

a) Polished surface of facies F1 (evaporite solution collapse breccia), with a corresponding photomicrograph (transmitted light, plane-polarized) showing clasts (Cl.) and an important porosity (blue) in the matrix (Ma.) of these breccia.

b) Field photography of a mudstone with root traces (facies F2).

c) Polished surface showing a flat-pebble conglomerate corresponding to the reworking of the facies F3 (algal laminite facies).

d) Transmitted light plane-polarized photomicrograph, showing light and dark undulating alternations corresponding to the algal laminites of facies F3.

e) Field photography of oscillation and current ripples in the facies F4 (intraclastic dolowackestone).

f) Field photography of escape burrow in the facies F4 (intraclastic dolowackestone).

- facies F4 (bioturbated dolowackestone);
- facies F5, a well-sorted oolithic grainstone, formed of more than 70% of ooids *(Fig. 5a)*, showing cross-bedded laminations and common erosive bases;
- facies F6, a bioclastic grainstone to packstone, poorly sorted, with lens shape geometries, showing brachiopods, crinoids and oyster fragments, commonly micritized *(Fig. 5b)*. Hummocky Cross Stratifications (HCS) have been observed in some of these lenses.

A typical sequence may show either facies F5 or F6 at its base. These two facies pass upward to facies F4 and/or F3, that are eroded at their top by the subsequent cycle *(Fig. 3b)*.

3.1.2.2 Interpretation

The well-sorted oolitic grainstone is interpreted as shoals deposited and migrating in a shallow-water subtidal environment (Halley *et al.*, 1983), as 2D-3D mobile sand dunes. Bioclastic packstone to grainstone lenses may be related to storm processes (presence of HCS), that seems to affect this shallow subtidal to intertidal environment. Bioclasts may have been transported from the adjacent subtidal environment, as they point to more open marine conditions. The intense micritization of these grains may point to a deposition in a shallow, low-energy environment where microborers and micro-organisms lived (Tucker and Wright, 1990). The biological escape structures in F4 likely reflect quick deposition after high hydrodynamic events such as storms particularly effective in an intertidal environment (Tucker and Wright, 1992).

These shallow subtidal to intertidal facies sequences correspond to shallowing-upward trends due to the filling of available space created by a positive accommodation.

3.1.3 Deep Subtidal Facies Sequence

3.1.3.1 Description

The deep subtidal facies sequence includes five facies. Facies F5 and F6 (described above) are present. The facies F7 is a poorly-sorted rudstone to grainstone, mainly composed of intraclasts, oncoids and peloids and subordinate crinoids *(Fig. 5c, d)*. The facies F8 *(Fig. 5e)* is supposed to be (as it is generally extensively dolomitized) originally a crinoidal wackestone, associated to peloids, brachiopods (*Spirifera*) and solitary corals (*Rugosa Zaphrentis*). Burrows at tops of beds and rare stratiform cherts have been observed. The facies F9 is a dolomudstone *(Fig. 5f)* with rare brachiopods (*Spirifera*), crinoids and solitary corals and exhibiting an intense bioturbation.

This facies sequence is generally composed at its base by the facies F8 or F9. Within these two facies, lenses of grainy facies with erosive bases (facies F5, F6 and F7) gradually appear with a thickening-upward trend, finally forming relatively continuous beds *(Fig. 3c)*.

3.1.3.2 Interpretation

The bioturbated dolomudstone (F9) is interpreted to be deposited in the deepest subtidal environment below the storm wave base (open shelf), as it presents a muddy texture and no sedimentary structures. Facies F8 is interpreted as an initial bioclastic and bioturbated wackestone deposited in a subtidal, low energy environment (muddy texture). The fauna (brachiopods, crinoids) points to open marine conditions (Flügel, 2004). This facies has been subsequently dolomitized. Oncoid and crinoid fragments observed in F7 are interpreted as reworked material in high-energy setting probably resulting from storm events. The association of facies F5, F6 and F7 may be considered as hydraulic dune complexes in a deeper subtidal environment, above storm wave base. In this setting, F8 may have been deposited in a low-energy environment compared to F6 or F7, at the bottomset of the dune complexes, where bioturbation can occur.

These facies sequences correspond to shallowing-upward trends. As the available space is only partially filled (no emersion at the top of sequences), it is not necessary to invoke changes in accommodation as origin for this facies sequence. The vertical stacking of these subtidal facies sequences, within the first third-order depositional sequence (Little Bighorn Member), shows a clear thickening-up and coarsening-up of facies F9 to F7. This may reflect a general migration of a granular facies belt into a fine facies belt (muddy depression). Such migration of granular bodies could be the result of internal processes within the basin, such as storms.

3.2 Synthetic Facies Model

In order to constrain the facies distribution and relationships, which are important parameters for the facies simulation, we have proposed a conceptual depositional model, based on the facies interpretation. Each facies is positioned on a proximal-distal depositional profile, which will enable to assess the vertical variation of depositional environment for each section *(Fig. 6a)*. Large-scale vertical trends have thus been assessed by the recognition of major sedimentary surfaces (erosional surfaces, hardgrounds, and solution-collapse breccias) and the vertical variation of depositional environment *(Fig. 6b)*. They correspond to variations of accommodation, assimilated to the third order sequences defined by Sonnenfeld (1996). Because of the very shallow depositional setting, the maximum flooding surfaces are not easily recognizable. Therefore, the maxima of decrease of bathymetry are used as sequence boundaries and also as reference surfaces to assess the general geometry (depositional profile) and to create the surface model prior to the simulations.

The depositional profile roughly corresponds to a carbonate ramp (sequences 1 and 2) evolving towards the most inner part of a flat-top platform during sequence 3 (Barbier, 2008). In the ramp, a large intertidal domain dominated by muddy,

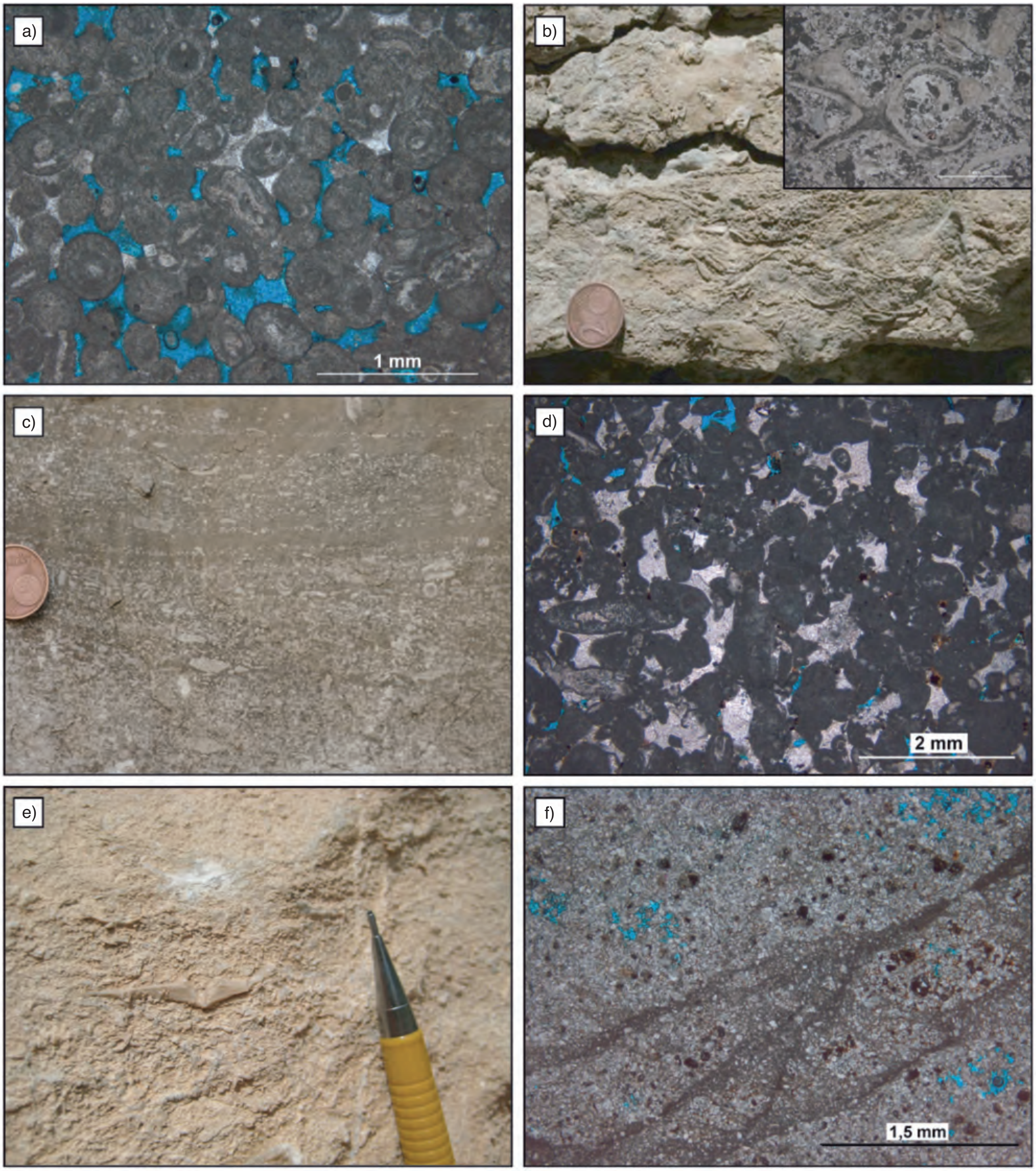

Figure 5
a) Transmitted light plane-polarized photomicrograph of the facies F5 (oolitic grainstones). Ooids are micritized.
b) Field photography and corresponding transmitted light plane-polarized photomicrograph of the facies F6 (bioclastic grainstone/packstone). Bioclasts consist mainly of brachiopods and crinoids. The matrix is partially dolomitized.
c) Field photography of the facies F7 (low angle, cross-bedded rudstone). Matrix is dolomitized whereas grains (crinoids, brachiopods, oncoids and ooids) are still calcite (white grains on the picture).
d) Transmitted light plane-polarized photomicrograph of an intraclastic grainstone (facies F7) cemented by a late stage sparry calcite. Primary porosity in blue.
e) Field photography of the facies F8 (crinoidal dolowackestone with brachiopod *Spirifera*).
f) Transmitted light plane-polarized photomicrograph of the facies F9 (dolomudstone). This facies is highly dolomitized and porous (13 to 17%), but beds are compartmentalized by shear band zone destroying porosity in few centimeters.

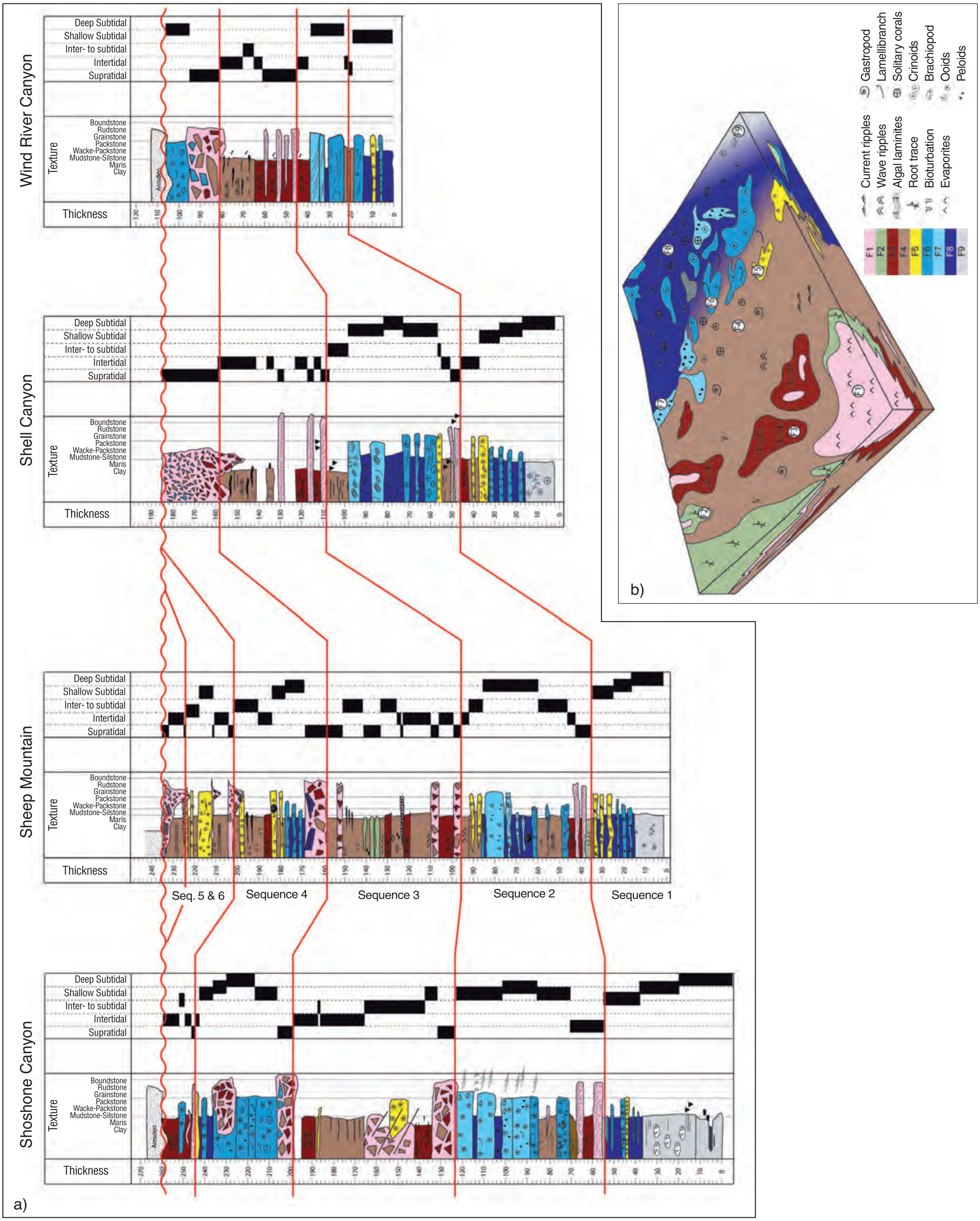

Figure 6

a) Basin-scale correlation transect, integrating the different sections used for the sedimentary (and diagenetic) characterization phase.

b) Associated conceptual depositional model. Colour code refers to the facies classification.

dolomitized facies (F3 and F4) developed in which carbonate sand bodies migrated (F5) (evidenced by coarsening-up subtidal facies sequence). The distal evolution of this domain is marked by subtidal muddy facies (F8, F9). The third sequence, which is very homogeneous from a sedimentological point of view, is deposited in the inner-part of a flat-top platform dominated mostly by intertidal and supratidal facies (F1 to F4). The mid and outer part of this platform is not represented in the studied area, being localized further North.

4 DIAGENETIC PHASES IDENTIFICATION

Several authors have already addressed the topic of the diagenetic history of the Madison Formation. A complete description and discussion of the origin and timing of the different diagenetic phases can be found in Katz *et al.* (2006) or Smith *et al.* (2004). As this paper is focused on the early diagenesis modeling (mainly because of the direct link between sedimentary facies and early diagenesis) only the early diagenetic phases will be described here.

4.1 Micritization

Bioclast micritization is common in the grainstone facies and is the earliest stage of the paragenetic sequence. Micrite envelopes (5 to 100 μm thick) mostly developed around crinoid clasts, bivalve shells and ooids *(Fig. 7a)*, and are attributed to micro-borer organisms living at or near the sediment–water interface (Purser, 1980).

4.2 Isopachous Bladed Rims

This cement occurs mainly in the oolithic grainstone facies and consists of a thin isopachous fringes around grains (5-20 μm thick). The fringes are formed by calcitic isopachous bladed crystals *(Fig. 7b)*. These rims are dull orange in cathodoluminescence and are non-ferroan. Isopachous cements are located in the whole grainstone layer, without any gradient of cementation (from the top to the base for example). Such early cements are common in shallow carbonate platforms and are interpreted as typical cement of a marine phreatic realm (Moore, 2001; Purser, 1969).

4.3 Syntaxial Cement

These cements are mainly observed as overgrowths (50 μm to up to 2 mm) around crinoid fragments and preferentially occurred in bioclastic grainstones and packstones. They are composed of inclusion-rich, non-ferroan crystals, showing frequently cleavage twins.

Under cathodoluminescence, three concentric zones alternating dull orange and non-luminescent layers are observed *(Fig. 7c)*. Isotopic data for the first zone (that have been separately sampled; *Fig. 8*) fall in the same range of values ($\delta^{18}O$ between −4.58‰ to −0.76‰; and $\delta^{13}C$ between 3.10‰ to 5.89‰) than oyster samples and than the estimated Mississippian marine calcite values (Veizer *et al.*, 1999). The isotopic values and petrographic characteristics (turbid crystals) of this first zone point to a formation in a marine phreatic environment. On the contrary, the two subsequent zones are limpid and have depleted isotopic data compared to the first zone. These data suggest a formation during the post-mississippian karst in a phreatic meteoric realm, under shallow burial conditions (Moore, 2001).

4.4 Early Lithification of Micrite

Mudstone facies may also show an early lithification without dolomitization processes. It is the case of facies F2, which shows a limestone lithology. The presence and the preservation of root traces suggest an early lithification associated to a supratidal environment. The processes of early lithification remain unclear as no specific structures are observed.

4.5 Early Dolomitization

In non-grainy facies, eogenesis is expressed by dolomitization processes rather than calcite cementation. Two types of dolomites crystals are observed. The first one is a dolomicrite (4-10 μm,) to dolomicrosparite (10-35 μm), with unimodal replacement fabric. It shows a dull red luminescence (in sequence 3) to non-luminescence (sequences 1 and 2) and is interpreted as occurring in supratidal and intertidal facies *(Fig. 7d)*. Isotopic values fall in the range of Mississippian marine dolomites ($\delta^{18}O_{PDB}$ between 0.5‰ to 5‰ and $\delta^{13}C_{PDB}$ between 1‰ to 4‰; *Fig. 8*).

The second type is an unimodal dolosparite selectively replacing the muddy matrix in subtidal bioclastic wackestone and packstone facies *(Fig. 7e)*. Dolomite crystal sizes range from 60 μm to 200 μm, they have cloudy core and show a mottled red-orange luminescence. They always exhibit a limpid and red luminescent dolomite overgrowth *(Fig. 7f)*. Moreover, dolomite oxygen values are lightly shifted towards lower values compared to Mississippian marine dolomites ($\delta^{18}O_{PDB}$ between −0.21‰ to −2.49‰ and $\delta^{13}C_{PDB}$ between 2.34‰ to 4.52‰; *Fig. 8*).

Whatever the type of dolomite, some ghost textures in rhombs are displaced relative to grains into packstones, reflecting an early pre-compaction, formation of these dolomites (Tucker and Wright, 1990). According to the isotopic data, the dolomicrite to dolomicrosparite is interpreted as linked to marine water, in an evaporative supratidal environment, as they are associated to supratidal facies, rich in evaporite pseudomorphoses. The dolosparite corresponds to the dolomitisation of subtidal facies, some of them being open marine facies. Rather than an evaporative

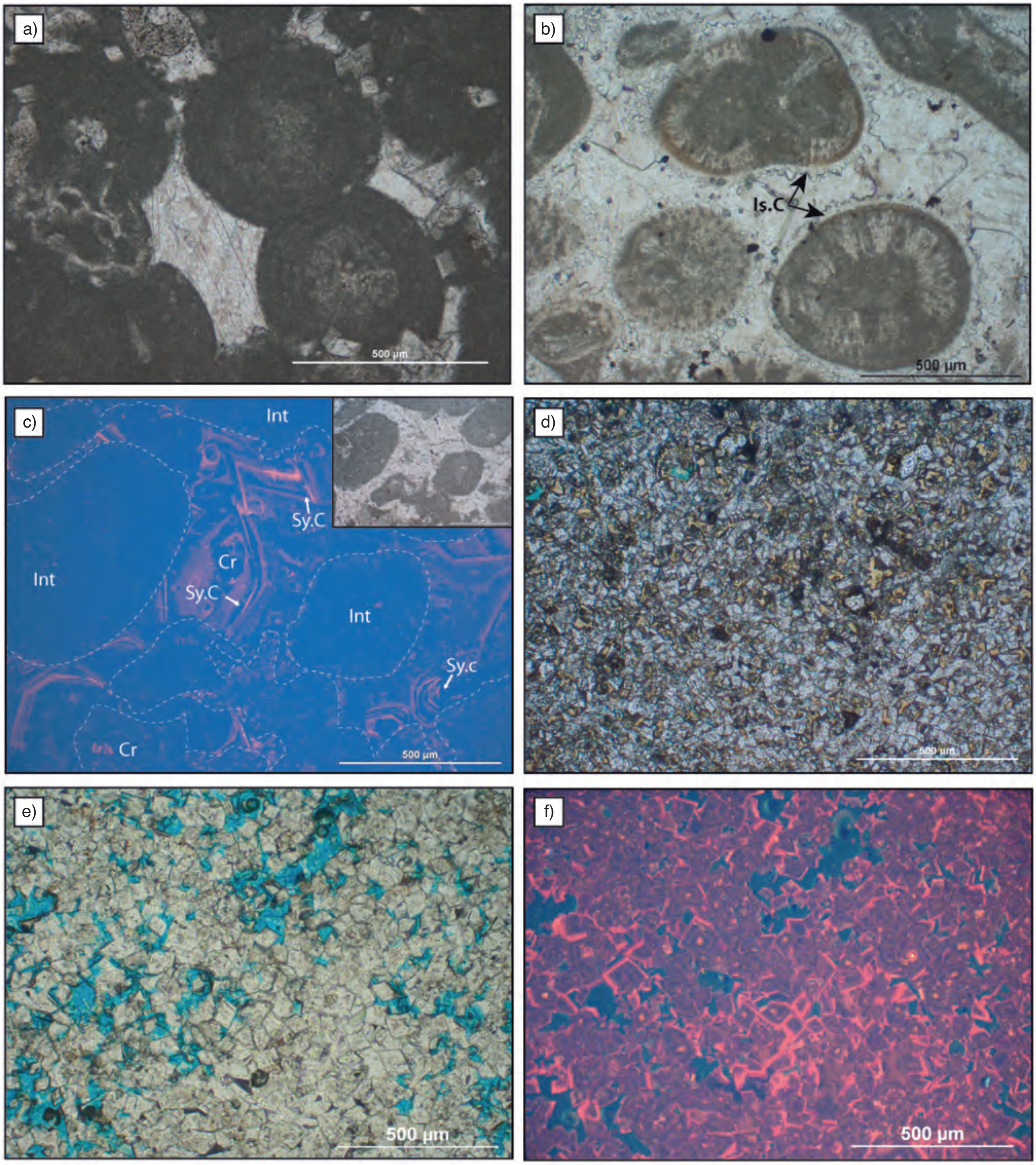

Figure 7

a) Transmitted light plane-polarized photomicrograph of an oolitic grainstone, showing an intense micritization of the cortex of ooids.

b) Transmitted light plane-polarized photomicrograph of an oolitic grainstone. Ooids are coated by a 15 µm thick isopachous calcite cement (Is.C).

c) Transmitted light plane-polarized and corresponding cathodoluminescence photomicrograph of an intraclastic (Int) grainstone with crinoids (Cr). Syntaxial calcite cement (Sy.C) shows very fine concentric dull orange zonations.

d) Transmitted light plane-polarized photomicrograph of a dolomicrosparite (10-30 µm crystal size), with unimodal replacive fabric.

e) Transmitted light plane-polarized photomicrograph of a dolosparite showing unimodal planar dolomite crystals, with sizes ranging from 30 to 50 µm.

f) Corresponding photomicrograph under cathodoluminescence. Dolomite crystals exhibit a dull orange first dolomite core with concentric zonations and a red luminescence overgrowth.

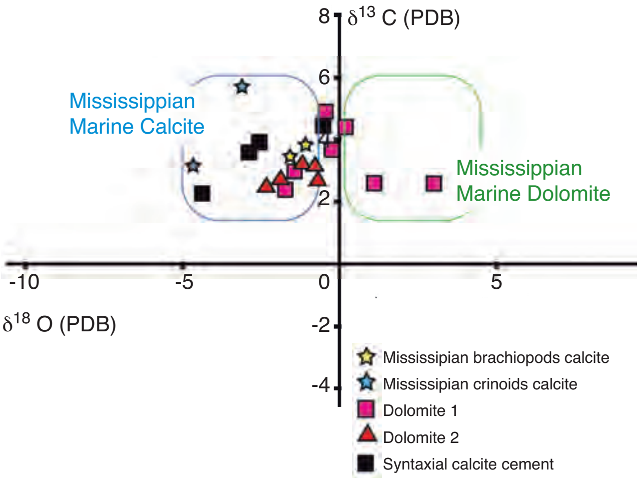

Figure 8

Cross-plot diagram of carbon and oxygen isotopic compositions of the early diagenetic phases. Mississippian marine calcite values are from Veizer *et al*. (1999). Mississippian marine dolomite are from Prokoph *et al*. (2008).

model, a seepage-reflux origin is proposed for the dolosparite formation, with a reflux that is directly related to overlying sabkha environments. Indeed, the dolomitization may occur quite early in this scenario, and the growing dolomites are expected to have relatively more depleted δ^{18}O values compared to sabkha dolomicrites. Moreover, with continuous dolomitization and recrystallization (evidenced by the mottled appearance and overgrowth), the dolomites tend to become coarser (60 to 120 μm) and their isotopic values tend to be reset or simply shifted related to the initial composition. Finally, strontium isotopic values (0.7083-0.7085), measured by Katz *et al*. (2006) on the same phase, differ from Mississippian marine values (0.7080-0.7082) and also support a recrystallization during the subsequent phase of diagenesis (Machel, 1997; Smith and Dorobek, 1993).

4.6 Diagenetic Imprints

For modeling purposes, seven "diagenetic imprints" have been elaborated. A diagenetic imprint is a succession of diagenetic phases that can coexist in the same sedimentary facies *(Fig. 9)*. For example, the diagenetic imprint D3 includes an important micritization of grains and the presence of rare syntaxial cement, associated with a partial dolomitization of the matrix. Thus, each sedimentary facies can be affected by various diagenetic imprints, in various proportions (based on petrographic analysis). For example, sedimentary facies F6 shows diagenetic imprints D2 (with a proportion of 60%) and D3 (with a proportion of 40%). These associations' rules are defined for each facies, and for each unit *(Tab. 2)*.

5 THREE DIMENSIONAL MODELING

5.1 Modeling Workflow

The previous dataset has been used for stochastic modeling with an in-house "IFP Energies nouvelles" software. This software is designed to respect sequence stratigraphic

Diagenetic phases	Diagenetic imprints D1	D2	D3	D4	D5	D6	D7
Early lithification				XX			XX
Dolomitization (dolomicrite)				XX	XX	XX	
Grain micritization	XX	XXX	XXX				
Isopachous calcite rims	XXX						
Syntaxial calcite cement	X	XXX	X		XX		
Dolomitization (dolosparite)			XX		XX	XX	

a)

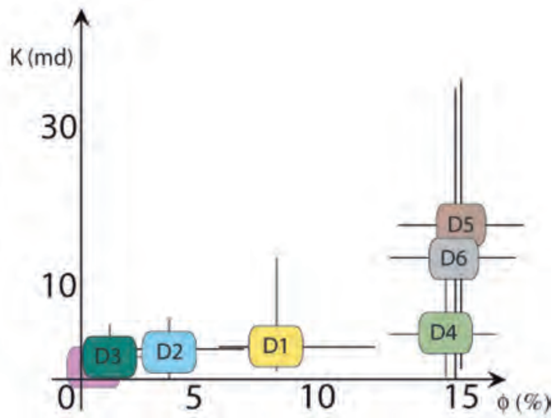

b)

Figure 9

a) Diagenetic imprints, grouping a succession of early diagenetic phases, used for the geostatistical simulations (X: low occurence; XX: average occurence; XXX: high occurence).

b) Ranges of petrophysical properties for each diagenetic imprint (whatever the sedimentary facies).

TABLE 2

Quantified associations' rules defining the diagenetic imprints observed for each facies within each unit

	F1	F2	F3	F4	F5	F6	F7	F8	F9
Unit 3									
D1									
D2									
D3									
D4	F1-D4 (100%)		F3-D4 (85%)	F4-D4 (55%)					
D5			F3-D5 (15%)	F4-D5 (45%)					
D6									
D7		F2-D7 (100%)							
Unit 2									
D1					F5-D1 (100%)				
D2						F6-D2 (60%)	F7-D2 (40%)		
D3						F6-D3 (40%)	F7-D3 (60%)	F8-D3 (5%)	
D4	F1-D4 (100%)		F3-D4 (80%)	F4-D4 (20%)					
D5			F3-D5 (20%)	F4-D5 (80%)				F8-D5 (90%)	
D6								F8-D6 (5%)	
D7		F2-D7 (100%)							
Unit 1									
D1					F5-D1 (100%)				
D2						F6-D2 (45%)			
D3						F6-D3 (55%)			
D4			F3-D4 (66%)	F4-D4 (25%)					
D5			F3-D5 (34%)	F4-D5 (75%)				F8-D5 (98%)	
D6								F8-D6 (2%)	F9-D6 (100%)
D7									

constraints and to honor both the well data themselves and their spatial variability. The model is 66 km long for 60 km wide, with a mean cell size of 1 km by 1 km horizontally and 60 cm high. The grid used for the simulation is divided vertically into three units, corresponding to the three studied depositional sequences. A proportional layering is used for units 1 and 2 and a "parallel-to-the-top" layering for unit 3.

In the present study, the simulation workflow is based on both plurigaussian and nested methods. Each step of the workflow presented in Figure 10 is performed sequentially. The sedimentary facies simulation was achieved using a plurigaussian algorithm (non-stationary simulation), constrained with the 5 sedimentary sections. It allows dealing with complex spatial relationships between lithotypes that result from different processes (through "lithotype rules"), and to include more geologic information.

The diagenetic imprint simulations were done independently, using a nested algorithm. In this approach, each diagenetic imprint is simulated within each sedimentary facies, based on the association rules defined in Table 2, and using the Sequential Indicator Simulation method (SIS). The main SIS parameters are probability distribution laws calibrated from data analysis and variograms. The latter express the spatial continuity of the properties and are the same that for the previous plurigaussian simulation, expressing the strong control of depositional facies on the diagenetic imprint. Finally, the different realizations (sedimentary facies and diagenetic imprints) are combined, to produce the joint simulation of both sedimentary facies and associated diagenetic imprints *(Fig. 10)*.

5.2 Choice and Representativity of the Geostatistical Parameters

The simulation parameters for the plurigaussian simulation (sedimentary facies simulation) were defined based on the outcrop analysis and the conceptual geological model. Main geostatistical parameters are:

- the Vertical Proportion Curves (VPC) and the matrix of proportions;
- the lithotype rules;
- the variogram models for the underlying Gaussian functions.

A VPC provides at each stratigraphic level, the proportion of each lithofacies (Dubrule, 1998). In other words, it represents the vertical succession and distribution of facies in one modeled unit (here a third-order sequence as simulations have been realized sequence by sequence). It is computed from well data, at each stratigraphic level. When the VPC is used as a parameter for the geological geostatistical simulations, the facies proportions are considered to be constant in average for each horizontal level (stationarity). The matrix of proportion corresponds to the cases when proportions vary also laterally (non stationarity, our case study). It is drawn as a 2D grid, each cell of which being a local vertical proportion curve (Doligez *et al.*, 2009; Ravenne *et al.*, 2000), and reproduces the spatial variability of facies trends. For each modeled unit (third-order depositional sequence), a matrix of proportion has been computed *(Fig. 10)*, based on 5 Vertical Proportion Curves (5 sedimentary sections) interpolated level by level with a kriging method.

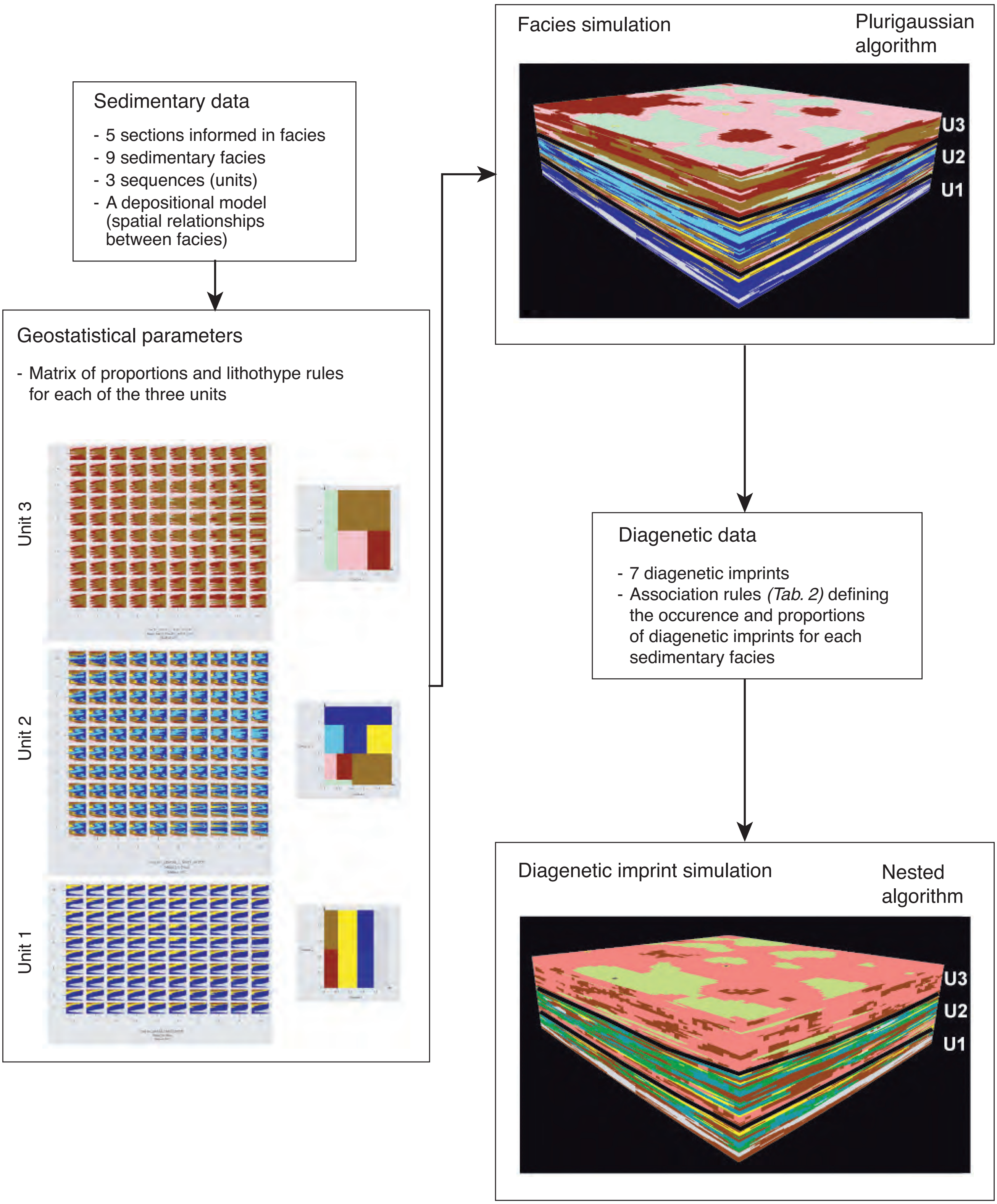

Figure 10

Modeling workflow used for the joint simulation of facies and diagenesis. See text for explanation.

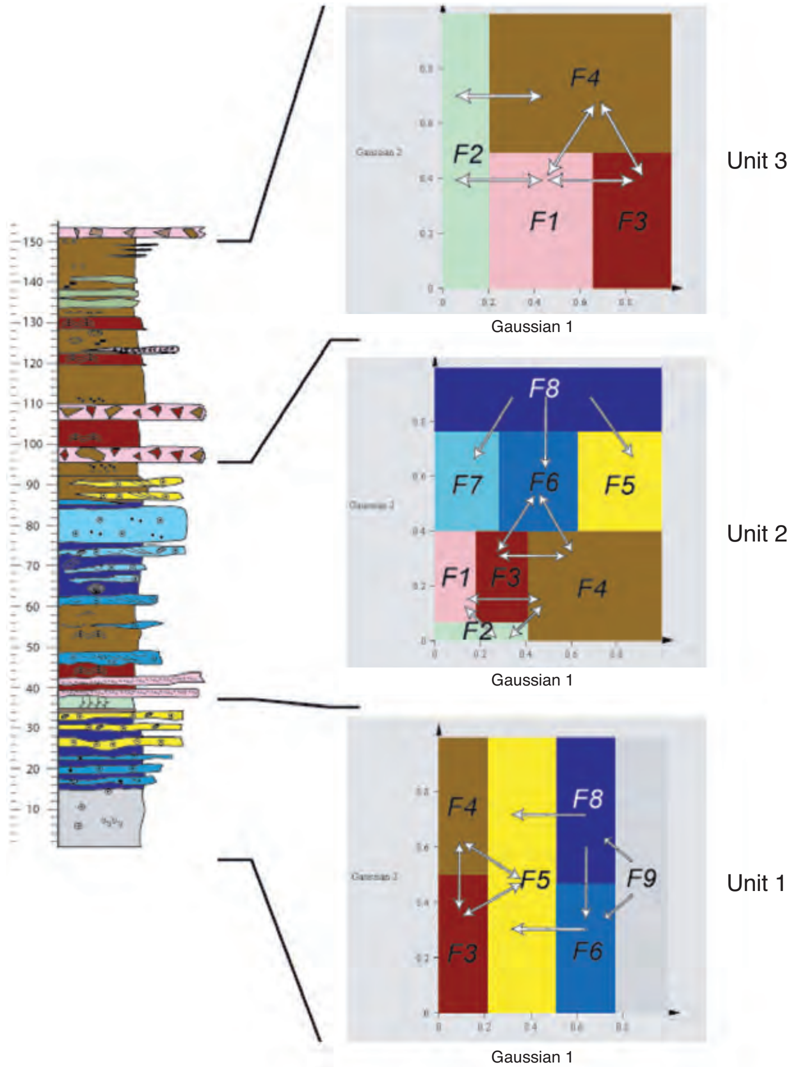

Figure 11

Lithotype rules proposed for each third-order depositional sequence (unit). See text for details.

Moreover, the plurigaussian algorithm requires that we define lithotype rules used together with the VPC as a facies substitution diagram, to reproduce the sequential and spatial organization of the sedimentary facies *(Fig. 3)*. Indeed, as already mentioned in the "sedimentological characterization" part of this article, the three studied third-order depositional sequences represent an evolution of the depositional profile, from a ramp system dominated by open-marine facies (sequence 1) to the most inner part of a flat-top platform (sequence 3), the second sequence being an intermediate case. Among the different potential lithotype rules, the most suitable representation of the geological model has been chosen. The number and the spatial distribution of facies are different from a sequence to another. It was therefore necessary to propose one lithotype rule for each third-order depositional sequence (modeled unit), to take this evolution into account *(Fig. 11)*.

In unit 1 *(Fig. 11)*, subtidal and shallow subtidal to intertidal facies sequences are observed. The lithotype rule respect firstly the facies succession of the subtidal sequence. Indeed, the subtidal mudstone (F9) can evolve either into the crinoidal wackestone (F8) or into the bioclastic grainstone to packstone (F6). The two latter facies can be themselves capped by the oolitic grainstone (F5). The shallow subtidal to intertidal shoal facies sequences is also represented by this lithotype rule as the facies F5 may evolve into the wavy dolostone (F4) or the laminite facies (F3).

The lithothype rule for the unit 2 *(Fig. 11)* is more complicated. Indeed, the three facies sequences, present in the unit should be respected. The supratidal facies sequence showing the transition of the wavy dolostones (F4) to stromatolithes (F3) and capped either by the evaporite solution collapse breccias (F1) or the mudstone with root traces (F2), is well illustrated by the gaussian 1. The two other facies sequences are represented by the second gaussian and follow the same arrangement than in unit 1.

As the unit 3 is only composed of intertidal to supratidal facies sequences, only four sedimentary facies existed coevally. The lithotype rule *(Fig. 11)* applied for this unit is simpler and shows that wavy dolostones (F4) and evaporite solution collapse breccias (F1) can be directly in relation with the three other facies. F4 being the most widespread facies and the basal facies of each cycles, it has been represented in bigger proportion in this lithotype rule.

At last in the plurigaussian algorithm (Le Loc'h and Galli, 1996; Thomas *et al.*, 2005), the facies simulations are performed using two stationary Gaussian Random Fields (GRF), which are truncated using local thresholds computed from the lithotype rule updated with the local proportions. Each Gaussian field imposes its spatial correlation structure to the facies, according to the defined threshold rule. These spatial structures corresponding to the variograms of the Gaussian functions are related to the spatial structures of the indicator functions of the facies through a complex relationship also using local proportions of each facies. In this study, we have used gaussian models for the two Gaussian Random Fields, in order to generate smooth distributions of the facies. Range distances for each gaussian used in our simulations are summarized in Table 3. They correspond to distances of maximum correlation and can be considered as maximum dimensions of the sedimentary bodies. Thus, range distances vary from 5 to 16 km in the horizontal directions and some meters along the vertical one *(Tab. 3)*, to be consistent with the continuity of the geological facies.

The simulation parameters for the nested simulation (diagenesis simulation) are dependant of the previous ones, as each diagenetic imprint is simulated within each sedimentary facies, based on the association rules *(Tab. 2)*. Thus, the variogram models for the diagenesis simultation are similar to those used for the facies simulation.

TABLE 3

Range distances for each gaussian used for the plurigaussian simulations (sedimentary facies)

	Unit 1		Unit 2		Unit 3	
Structure used	Gaussian 1	Gaussian 2	Gaussian 1	Gaussian 2	Gaussian 1	Gaussian 2
Range 1 x - (km)	13.1	16.5	13.1	16.5	5.2	5.2
Range 2 y - (km)	13.1	16.5	13.1	16.5	5.2	5.2
Range 3 z - (m)	2.5	2.5	2.5	5	5	5

5.3 Results and discussion

5.3.1 Simulation Results

The joint simulation, both of facies and diagenesis, illustrates in three dimensions the extension and distribution of the different facies and heterogeneities occurring in each modeled unit (homologous to 3rd order depositional sequence). In our workflow, only the early diagenesis has been modeled. However, the general paragenesis established for the Madison Formation (Smith *et al*., 2004; Westphal, 2004) has shown that the mesogenetic phases are very scarced and poorly developed in the Sheep Mountain area. Thus, our joint simulation may reflect correctly the potential reservoir, even if only the eogenetic phases have been simulated. Figure 12 presents one example of simulation in facies and diagenesis for each of the three modeled units. Moreover, sequences 1 and 2 are divided into two parts: retrograding and prograding trends. As the sequence 3 is mainly aggrading, no distinction between retrograding and prograding part are shown.

5.3.2 Validation of the Simulations

The simulation results were validated by comparison with the conceptual geological model based on the field and petrographic observations described above.

In sequence 1 *(Fig. 13)*, the retrograding part exhibits a homogeneous sedimentation pattern, dominated by facies F8 and F9 (bioclastic wackestone and mudstone). The prograding part of this sequence is dominated by oolithic sand dunes facies (F5), muddy peritidal facies in the inner setting (F3/F4) and open-marine facies (F8/F9), organized in deep subtidal facies association. This facies distribution is well reproduced in the stochastic facies simulation *(Fig. 12)*: indeed, the base of the sequence shows large spatial extension and a homogeneous distribution of facies (F8 and F9), whereas the top part is more heterogeneous: indeed muddy facies are discontinuous, being separated by laterally connected sand dunes. In terms of diagenesis, the simulation seems to correctly honour the geological concepts as well: the peritidal facies (dolomicrite to microsparite) are mainly affected by the diagenetic imprint D4, whereas the subtidal facies that show a dolosparite texture, are correspondingly affected by the diagenetic imprints D5 and D6. Oolithic dune facies may act as barriers as they are cemented early (mainly by an isopachous rim cement), represented in the simulation by the diagenetic imprint D1 that considerably decreases their petrophysical properties *(Fig. 9b)*. To sum it up, in this sequence, the potential reservoir distribution is strongly controlled by

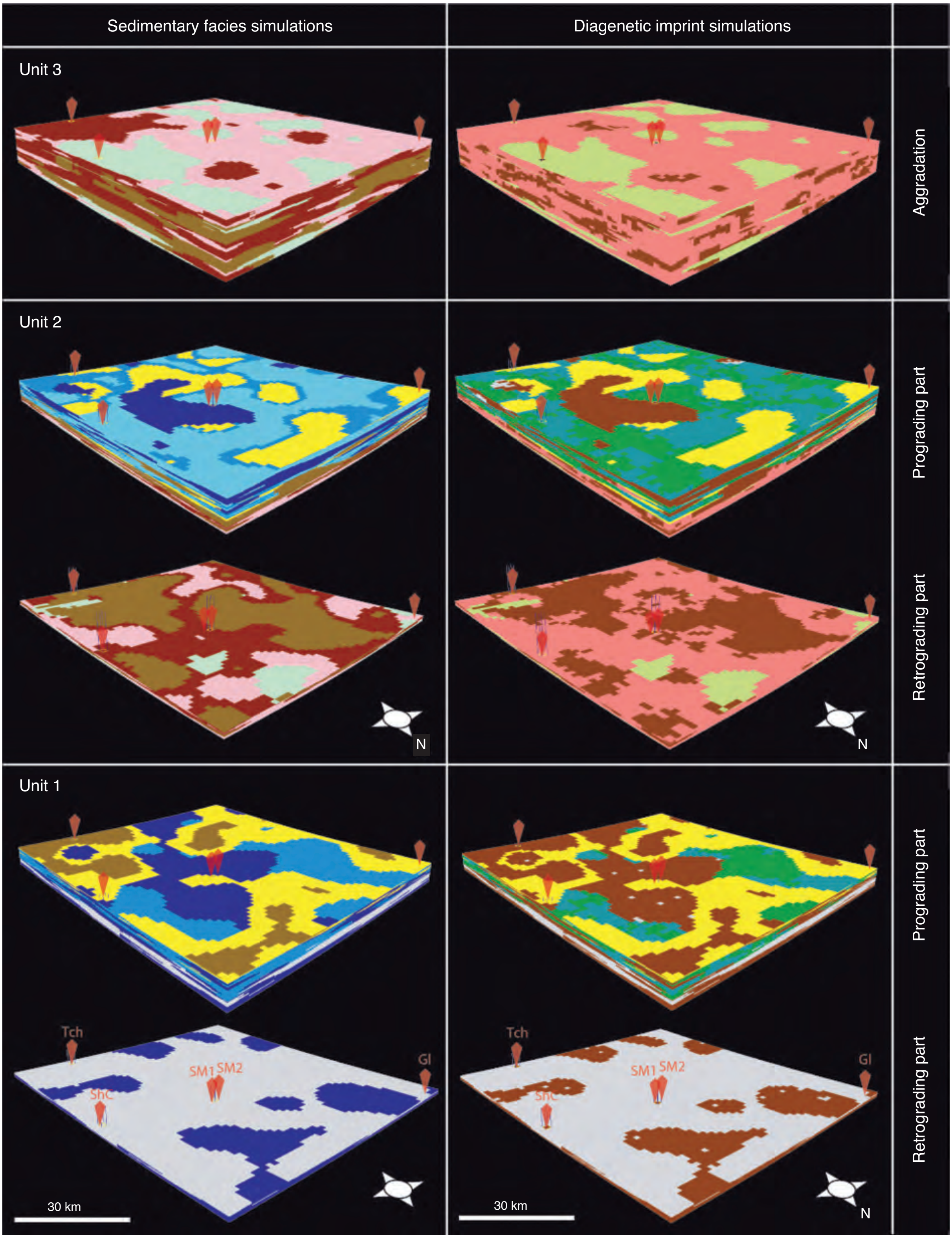

Figure 12

Simulation results for each modeled unit (depositional sequence). The figure shows a realization in facies and diagenesis for each part of the sequence (retrograding and prograding). As the sequence 3 is mainly aggrading, no distinction between retrograding and prograding part are shown. Note the sections used for simulation (SM1 and SM2: Sheep Mountain backlimb and forelimb; ShC: Shell Canyon; Gl: Garland Field; Tch: Torchlight Field). Colour code in Table 2.

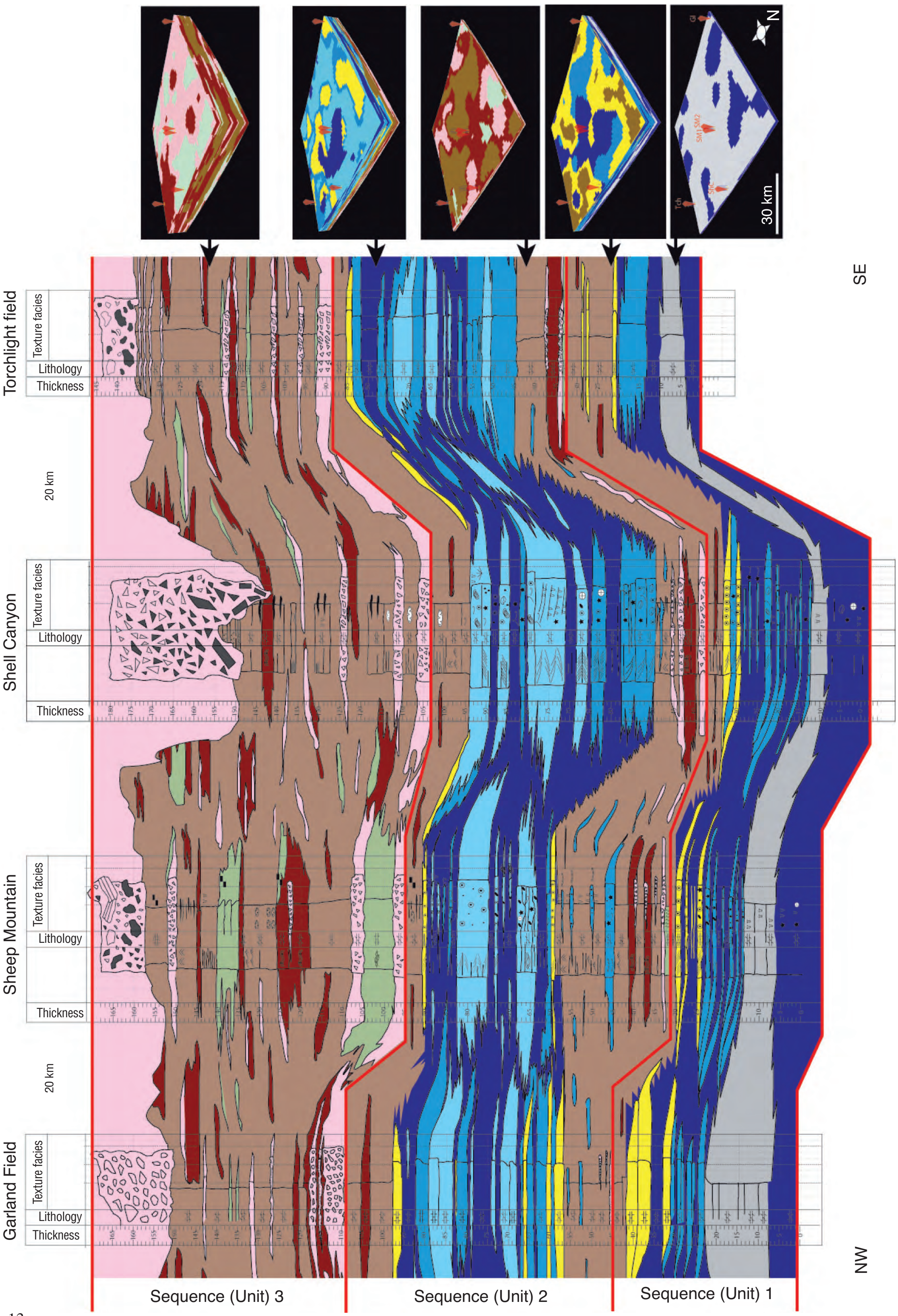

Figure 13

Correlation transect between the sections used as constraints for modeling, showing the supposed lateral continuity of the sedimentary bodies (color code in *Fig. 6*). This transect is compared with each of the geostatistical simulation of Figure 12. Note the consistency between the two approaches.

the sedimentary facies distribution. However, the diagenetic imprints may strongly decrease reservoir properties of some facies (such as sand dune facies, where average porosity is 8%, and permeability less than 5 mD) that might have been good reservoirs (good primary porosity, plugged by D1 overprint).

In sequence 2 *(Fig. 13)*, the retrograding part is dominated at its base by homogeneous peritidal facies (F2 to F4), showing a large spatial and vertical extension. Moreover, they show a dolomicrite to dolomicrosparite texture, which give them good potential petrophysical properties *(Fig. 9b)*. The upper part of the sequence is again much more heterogeneous with discontinuous small scale (a few kilometers) oolithic sand dunes (F5), bioclastic storm beds (F6) and open-marine facies (F7 and F8). These three last facies also exhibit variability in term of diagenetic imprints that increase the heterogeneity of this part of the series. In this case, potential reservoir distribution is strongly altered by the diagenetic imprint. Facies and diagenesis simulations for unit 2 *(Fig. 12)* are coherent with this conceptual geological scheme. Indeed, the simulations for the base of the unit show a patchy distribution of peritidal facies (typical of this kind of environment and in agreement with our depositional model, *Fig. 6b)*. These facies are mainly affected by the diagenetic imprints D4 and D5 (associated to dolomicrosparite texture). The diagenesis variability in the upper part of the unit is also well reproduced *(Fig. 12)*.

Finally, the third depositional sequence is characterized by an aggradational trend *(Fig. 13)*, dominated by patchy peritidal facies (F1 to F4). However, major parts of these facies are dolomitized (dolomicrite to dolomicrosparite), which tend to smooth the facies heterogeneity and increase the petrophysical properties, by a dolomitization process. (average porosity is 15%, permeability between 5 and 15 mD, *Fig. 9b*). Barriers correspond to F2 facies (early lithified mudstone) associated to locally emerged areas that are spatially limited. On the contrary to sequence 2, potential reservoir distribution is strongly improved by the diagenesis. The facies distribution is well reproduced in the stochastic facies simulation *(Fig. 12)* as the patchy distribution of peritidal facies is well rendered by a moderate spatial heterogeneity, coherent with the depositional model. In term of diagenesis, the simulation for unit 3 shows an homogeneous pattern, mainly dominated by diagenetic imprint D4 (associated to dolomicrosparite texture; *Fig. 12*). It should be mentioned here, that the main target exploited in Wyoming, in the Madison Formation is this unit 3, corroborating our approach.

CONCLUSION

This study first demonstrates our ability to account, during the reservoir modeling process, for both the heterogeneity in the sedimentary facies distribution, and in the subsequent imprint of diagenetic facies. Our study also shows the necessity to integrate the sedimentary and petrographic analysis in the modeling workflows. A thorough description and quantification of both facies and diagenetic phases are necessary inputs for a valid geostatistical modeling of the reservoir properties. It also shows the use of such coupled-simulation, as the diagenesis may completely modify the distribution of reservoir facies only based on a facies simulation.

However, the case that is treated in this article is limited to early diagenesis, as this latter is clearly controlled by palaeoenvironments and is directly linked to sedimentary facies. It enables and justifies the choice of the nested method for simulation purposes. It also implies to complete this approach with other modeling tools in the case of other types of diagenesis. For example, the superimposition of a fault-related diagenesis on an early diagenesis implies the use of deterministic approach or object-based methods.

We can now propose to extend such reservoir scale modeling by integrating fracture network simulations. Indeed, based on outcrop or well data, it is possible to characterize the quantitative joint network properties and to correlate them to the coupled sedimentary facies and diagenetic imprint. Based on such correlation it should be possible to simulate a Discrete Fracture Network (DFN) for each mechanical unit, and modify the hydraulic properties, later influencing the burial diagenesis as well.

ACKNOWLEDGMENTS

To Michael Joachimsky at the University of Erlangen – Germany (Institute of Geology and Mineralogy), for performing the stable isotopes analyses.

REFERENCES

Amrouch K., Lacombe O., Bellahsen N., Daniel J.M., Callot J.P. (2010) Stress and Strain patterns, kinematics and deformation mechanisms in basement-cored anticline: Sheep mountain Anticline (Wyoming), *Tectonics* **29**, 1-28.

Ayora C., Taberner C., Saaltink M.W., Carrera J. (1998) The genesis of dedolomites: a discussion based on reactive transport modelling, *J. Hydrol.* **209**, 346-365.

Barbier M. (2008) Étude de la relation fracturation/diagenèse dans un analogue de réservoir carbonaté: l'exemple de Sheep Mountain (Wyoming, États-Unis), *MSc Thesis*, Université Montpellier 2, France.

Blakey R.C. (2005) Paleogeography and Tectonic Evolution of Late Paleozoic Sedimentary Basins, Southwestern North America, *Annual Meeting of the Geological Society of America*, Salt Lake City, Oct. 2005, http://jan.ucc.nau.edu/~rcb7/RCB.html.

Caspard E., Rudkiewicz J.L., Eberli G.P., Brosse E., Renard M. (2004) Massive dolomitization of a Messinian reef in the Great Bahama Bank: a numerical modelling evaluation of Kohout geothermal convection, *Geofluids* **4**, 40-60.

Consonni A., Ronchi P., Geloni C., Battistelli A., Grigo D., Biagi S., Gherardi F., Gianelli G. (2010) Application of numerical modelling to a case of compaction-driven dolomitization: a Jurassic palaeohigh in the Po Plain, Italy, *Sedimentology* **57**, 209-231.

Dickson J.A.D. (1966) Carbonate identification and genesis as revealed by staining, *J. Sediment. Res.* **36**, 2, 491-505.

Doligez B., Beucher H., Pontiggia M., Ortenzi A., Mariani A. (2009) Comparison of Methodologies and Geostatistical Approaches for Diagenesis Quantification, *AAPG Convention*, Denver, Colorado, 7-10 June.

Dowd P.A., Pardo-Iguzquiza E., Xu C. (2003) Plurigau: a computer program for simulating spatial facies using the truncated plurigaussian method, *Comput. Geosci.* **29**, 123-141.

Dubrule O. (1998) *Geostatistics in petroleum geology,* AAPG Continuing Education Course Note Series, #38, AAPG.

Elrick M., Read J.F. (1991) Cyclic Ramp to Basin Carbonate Deposits, Lower Mississippian, Wyoming and Montana: A combined field and Computer modeling Study, *J. Sediment. Petrol.* **61**, 7, 1194-1224.

Emery X. (2007) Simulation of geological domains using the plurigaussian model: New developments and computer programs, *Comput. Geosci.* **33**, 1189-1201.

Flügel E. (2004) *Microfacies of Carbonate Rocks*, Springer, New York.

Gutschick R., Sandberg C., Stanley D., Moore G. (1983) Mississippian continental margins of the coterminous United States, in *The shelfbreak: critical interface on continental margins*, Stanley D.J., Moore G.T. (eds), SEPM Special Publication **33**, Tulsa, Oklahoma.

Haldorsen H.H., Damsleth E. (1990) Stochastic Modelling, *J. Petrol. Technol.* **42**, 4, 404-412.

Halley R.B., Harris P.M., Hine A.C. (1983) Back Margin Environment, in *Carbonates Depositional Environments*, Scholle P.A., Bebout D.G., Moore C.H. (eds), AAPG Memoir **33**, Tulsa, Oklahoma.

Hardie L.A., Shinn E.A. (1986) *Carbonate Depositional Environments; Part 3: Tidal flats*, Colorado School of Mines Quarterly **81**, Golden, Illinois.

Katz D., Eberli G., Swart P., Smith L. (2006) Tectonic-Hydrothermal brecciation associated with calcite precipitation and permeability destruction in Mississippian carbonate reservoirs, Montana and Wyoming, *AAPG Bull.* **90**, 1803-1841.

Labourdette R. (2007) 3D sedimentary modelling: toward the integration of sedimentary heterogeneities in reservoir models, *PhD Thesis*, Université Montpellier 2, France.

Lantuéjoul C. (2001) *Geostatistical simulation: models and algorithms*, Springer, Berlin.

Laubach S.E., Olson J., Gross M.R. (2009) Mechanical and fracture stratigraphy, *AAPG Bull.* **93**, 1413-1427.

Le Gallo Y., Bildstein O., Brosse E. (1998) Coupled reaction-flow modeling of diagenetic changes in reservoir permeability, porosity and mineral compositions, *J. Hydrol.* **209**, 366-388.

Le Loc'h G., Galli A. (1996) Truncated plurigaussian method: theoritical and practical point of view, in *Geostatistics Wollongong'96 Vol. 1*, Baafi E.Y., Schofield N.A. (eds), Kluwer Academic Publisher, pp. 211-222.

Machel H.G. (1997) Recrystallization *versus* neomorphism, and the concept of "significant recrystallization" in dolomite research, *Sediment. Geol.* **113**, 161-168.

Matheron G., Beucher H., de Fouquet C., Galli A., Guérillot D., Ravenne C. (1987) Conditional simulation of the geometry of fluvio-deltaic reservoirs, in *SPE Annual Technical conference and Exhibition*, Dallas, Texas, 27-30 September 1987, *SPE* 16753.

Moore C.H. (2001) *Carbonate reservoirs - Porosity evolution and diagenesis in a sequence stratigraphic framework*, Developments in Sedimentology **55**, Elsevier, Amsterdam.

Neely T.G., Erslev E.A. (2009) The interplay of fold mechanisms and basement weaknesses at the transition between Laramide basement-involved arches, north-central Wyoming, U.S.A., *J. Struct. Geol.* **31**, 9, 1012-1027.

Normando M.N., Remacre A.Z., Sancevero S.S. (2005) The Study of Plurigaussian Simulation's Lithotype Rule in Reservoir Characterization Process, *SPE Latin American and Caribbean Petroleum Engineering Conference*, Rio de Janeiro, Brazil, 20-23 June.

Olson J.E., Laubach S.E., Lander R.L. (2007) Combining diagenesis and mechanics to quantify fracture aperture distributions and fracture pattern permeability, in *Fractured reservoirs,* Lonergan L., Jolley R.J., Sanderson D.J., Rawnsley K. (eds), Geological Society of London Special Publication **270**, London.

Paterson R.J., Whitaker F.F., Smart P.L., Jones G.D., Oldham D. (2008) Controls on early diagenetic overprinting in icehouse carbonates: Insights from modelling hydrological zone residence times using CARB3D+, *J. Sediment. Res.* **78**, 258-281.

Poole F., Sandberg C., Stewart J., Stevens C., Fritsche A. (1977) Mississippian paleogeography and Tectonics of the western United States, in *Paleozoic paleogeography of the western United States*, Stewart J.H., Stevens C.H., Fritsche A.E. (eds), Pacific Section SEPM Symposium **1**, 67-85.

Prokoph A., Shields G.A., Veizer J. (2008) Compilation and time-series analysis of a marine carbonate $\delta^{18}O$, $\delta^{13}C$, $^{87}Sr/^{86}Sr$ and $\delta^{34}S$ database through Earth history, *Earth-Sci. Rev.* **87**, 3-4, 113-133.

Purser B.H. (1969) Syn-sedimentary marine lithification of middle Jurassic Limestones in Paris Basin, *Sedimentology* **12**, 205-230.

Purser B.H. (1980) *Sédimentation et diagenèse des carbonates néritiques récents (Tome 1)*, Publications de l'Institut français du pétrole **1**, Technip, Paris.

Ravenne C., Galli A., Doligez B., Beucher H., Eschard R. (2000) Quantification of facies relationships via proportion curves, *31st International Geological Congress*, Rio de Janeiro, 6-17 August.

Reid S., Dorobek S., Loucks R., Sarg J. (1993) Sequence stratigraphy and evolution of a progradational, foreland carbonate ramp, Lower Mississippian Mission Canyon Formation and Stratigraphic equivalents, Montana and Idaho, in *Carbonate Sequence stratigraphy. Recent developments & applications*, Loucks R.G., Sarg J.F. (eds), AAPG Memoir **57**, Tulsa, Oklahoma.

Rezaei M., Sanz E., Raeisi E., Ayora C., Vázquez-Suñé E., Carrera J. (2005) Reactive transport modeling of calcite dissolution in the fresh-salt water mixing zone, *J. Hydrol.* **311**, 282-298.

Rosenbaum J., Sheppard S.M. (1986) An isotopic study of siderites, dolomites and ankerites at high temperatures, *Geochim. Cosmochim. Ac.* **50**, 1147-1150.

Salas J., Taberner C., Esteban M., Ayora C. (2007) Hydrothermal dolomitization, mixing corrosion and deep burial porosity formation: numerical results from 1-D reactive transport models, *Geofluids* **7**, 99-111.

Sando W. (1988) Madison Limestone (Mississippian) Paleokarst: A Geologic Synthesis, in *Paleokarst*, Choquette P., James N. (eds), Springer-Verlag, New York.

Sando W.J., Bamber E.W. (1985) Coral zonation of the Mississippian System in the Western Interior Province of North America, *United States Geological Survey Professional Paper* **1334**, 3-64.

Shackleton J.R., Cooke M.L., Sussman A.J. (2005) Evidence for temporally changing mechanical stratigraphy and effects on vein-network architecture, *Geology* **33**, 101-104.

Smith L., Eberli G., Sonnenfeld M. (2004) Sequence stratigraphic and paleogeographic distribution of Reservoir quality Dolomite, Madison Formation, Wyoming and Montana, in *Integration of Outcrop and Modern Analogs in Reservoir Modeling*, Grammer G.M., Harris P.M., Eberli G.P. (eds), AAPG Memoir **80**, Tulsa, Oklahoma.

Smith T.M., Dorobek S.L. (1993) Alteration of early-formed dolomite during shallow to deep burial: Mississippian Mission Canyon Formation, central to southwestern Montana, *Geol. Soc. Am. Bull.* **105**, 1389-1399.

Sonnenfeld M.D. (1996) Sequence evolution and hierarchy within the lower Mississippian Madison Limestone of Wyoming, in *Paleozoic Systems of the Rocky Mountain Region*, Longman M.W., Sonnenfeld M.D. (eds), RMS-SEPM, Denver, Colorado.

Stanton H.I., Erslev E.A. (2004) Sheep Mountain Anticline: backlimb tightening and sequential deformation in the Bighorn Basin, Wyoming, *Wyoming Geol. Assoc. Guidebook* **53**, 75-87.

Steefel C.I., MacQuarrie K.T.B. (1996) Approaches to modeling of reactive transport in porous media, in *Reactive Transport in Porous Media*, Lichtner P.C., Steefel C.I., Oelkers E.H. (eds), *Rev. Mineral.* **34**, 83-125.

Tucker M., Wright P., Dickson J.A.D. (1990) *Carbonate Sedimentology*, Blackwell Science Ltd, Oxford.

Veizer J., Ala D., Azmy K., Bruckschen P., Buhl D., Bruhn F., Cardem G.A.F., Diener A., Ebneth S., Godderis Y., Jasper T., Korte C., Pawellek F., Podlaha O.G., Strauss H. (1999) ^{87}Sr / ^{86}Sr, $\delta^{13}C$ and $\delta^{18}O$ evolution of Phanerozoic seawater, *Chem. Geol.* **161**, 59-88.

Wachter E., Hayes J.M. (1985) Exchange of oxygen isotopes in carbon-dioxide phosphoric acid systems, *Chem. Geol.* **52**, 365-374.

Warren J.K. (2006) *Evaporites sediments, ressources and hydrocarbons*, Springer-Verlag, Heidelberg.

Wennberg O.P., Svånå T., Azizzadeh M., Aqrawi A.M.M., Brockbank P., Lyslo K.B., Ogilvie S. (2006) Fracture intensity vs. mechanical stratigraphy in platform top carbonates: The Aquitanian of the Asmari Formation, Khaviz anticline, Zagros, southwest Iran, *Petrol. Geosci.* **12**, 235-246.

Westphal H., Eberli G., Smith L.B., Grammer M., Kislak J. (2004) Reservoir characterization of the Mississippian Madison Formation, Wind River Basin, Wyoming, *AAPG Bull.* **88**, 4, 405-432.

Whitaker F., Smart P., Hague Y., Waltham D., Bosence D. (1997) Coupled two-dimensional diagenetic and sedimentological modeling of carbonate platform evolution, *Geology* **25**, 175-178.

Whitaker F., Smart P.L., Jones G.D. (2004) Dolomitization: from conceptual to numerical models, in *The Geometry and Petrogenesis of Dolomite Hydrocarbon Reservoirs*, Braithwaite C. Rizzi G., Darke G. (eds), *Geol. Soc. London Spec. Publ.* **235**, London.

Xiao Y., Jones D. (2006) Reactive Transport Modeling of Carbonate and Siliciclastic Diagenesis and Reservoir Quality Prediction, *Abu Dhabi International Petroleum Exhibition and Conference*, Abu Dhabi, UAE, 5-8 November, *SPE paper* 101669.

Final manuscript received in February 2011
Published online in October 2011